Design of sediment detention basins: Scaled model experiments and application

Anita Moldenhauer-Roth, Guillaume Piton, Sebastian Schwindt, Mona Jafarnejad, Anton Schleiss

Design of sediment detention basins: Scaled model experiments and application

Anita Moldenhauer-Roth[a,1,*], Guillaume Piton[b], Sebastian Schwindt[a,2], Mona Jafarnejad[a], Anton J. Schleiss[a]

[a]*Hydraulic Constructions Platform (PL-LCH), Swiss Federal Institute of Technology Lausanne (EPFL), Station 18, CH-1015 Lausanne, Switzerland*
[b]*Université Grenoble Alpes, Institut national de recherche en sciences et technologies pour l'environnement et l'agriculture (IRSTEA), UR ETNA, Grenoble, France.*

Abstract

Sediment detention basins are implemented on mountain rivers to trap solid material that may aggravate the flooding of downstream settlements. However, retention structures built in the past may unnecessarily retain sediment during non-hazardous flood events, resulting in high maintenance costs and sediment deficit downstream. In addition, the so-called spontaneous self-flushing of previously retained sediment during floods has occasionally been observed. Recent research suggests to design sediment detention basins for controlling sediment passage with a guiding channel across the deposition area upstream of a hybrid barrier. Such barriers consist of a check dam with a slot orifice and an upstream bar screen with a bottom clearance in order to benefit from a combined mechanical-hydraulic retention control. The present paper enhances this pioneering research with the help of new experimental data, including a wide range of sediment mixtures and large wood, as well as variable barrier heights. Improved design criteria are provided regarding the bar screen and the basin storage capacity. The functionality of the enhanced concept for sediment detention is illustrated by a case study on a physical model: the protection of the Villard-Bonnot village (France) against torrential hazards.

[*]Corresponding author

Email address: anita.roth@alumni.epfl.ch (Anita Moldenhauer-Roth)

[1]Present Address: Versuchsanstalt für Wasserbau (VAW), Eidgenössische Technische Hochschule, ETHZ, Hönggerbergring 26, HIA C53, Zürich, Switzerland

[2]Present Address: Institute for Modelling Hydraulic and Environmental Systems, University of Stuttgart, Pfaffenwaldring 61, 70569 Stuttgart, Germany

Keywords: Sediment continuity, Sediment trap, Bedload, Open check dam, Sediment flushing

1. Introduction

The sudden occurrence and the high capacity to mobilize and transport sediment characterize flood events of mountain rivers, which represent a serious danger for downstream settlements in alpine regions (Badoux et al., 2014). The fluvially transported sediment near the riverbed (bedload) is characterized by large amounts of gravel, cobbles, and boulders (Piton & Recking, 2017). River reaches on alluvial fans passing through settlements have a lower bedload transport capacity compared with upstream reaches due to lower gradients (longitudinal channel slope) and constrained width. The resulting difference in the transport capacity can cause sediment deposition with the consequence of flooding of urban areas (Hübl, 2018). Protection structures (so-called sediment traps or debris basins) upstream of settlements on alluvial fans are required to prevent channel obstruction by sediment, and also, large wood. Otherwise, settlements may experience severe floods and damages, including fatalities (Huebl & Fiebiger, 2005; Piton et al., 2017).

A sediment trap typically consists of a deposition basin, where the riverbed is widened and a lower slope is imposed, with a flow control structure (barrier or check dam) at the outlet (Zollinger, 1984). When the flow enters the deposition basin, the water spreads in the widened area. Thus, both the flow depth and the energy slope decrease in the deposition basin, which triggers sediment deposition. Undesired deposition of transported sediment at low discharges can be controlled with structural flow confinements inside the retention basin (Piton et al., 2018a; Schwindt et al., 2018). Flow control structures are permeable barriers, which are mostly referred to as (open) check dams in the literature. The sediment deposition in the vicinity of a flow control structure is either initiated through direct clogging of its openings (*mechanical control*) or delta formation under low flow velocities in the backwater of the structure (*hydraulic control*) (Armanini et al., 1991; Piton & Recking, 2016a). The individual application of either control mechanism for flood protection has drawbacks and advantages.

The reliability of mechanical control depends on the size of the transported sediment or large wood, but size estimates of expected sediment or wood (e.g., based on deposits from former floods) are associated with high uncertainty (Kaitna & Hübl, 2013; Shima et al., 2015, 2016). Mechanical control is preferable when the main objective is to retain coarse sediment and minimize the retention of fine sediment. Flow control structures in the shape of check dams using mechanical control have been used at least since the 1950s (Clauzel & Poncet, 1963; Reneuve, 1955). Such check dams typically incorporate small openings and/or are equipped with bar screens. Moreover, the design and performance of equivalent structures in Japan (so-called *Sabo dams*, made of steel pipes) use the mechanical control principle to capture debris and wood-laden flows only (Horiguchi et al., 2015; Horiguchi & Richefeu, 2020; Ikeya, 1989; Shima et al., 2015, 2016; Tateishi et al., 2020).

In Europe, other concrete structures with multiple openings (so-called *fins* or *breakers*) are also dedicated to trap only boulders or large wood (see e.g., Bergmeister et al., 2009).
Sediment deposition in the backwater of hydraulic control structures is driven by hydrodynamics (flow depth and velocity) (Schwindt et al., 2019). In this case, the size of trapped sediment is driven by the transport capacity in the deposition basin, where grain-size selective sediment sorting processes build a local alluvial cone during floods (Fedele & Paola, 2007). However, hydraulic control entails the risk of so-called undesired self-flushing of previously deposited sediment. Self-flushing is triggered by discharge and flow depth decreases, which cause the mobilization of sediment previously deposited in the deposition basin (Bezzola, 2008). Thus, hydraulic control is useful to alter flood and sediment transport peaks (Armanini & Larcher, 2001). Slit dams (i.e., barriers with openings experiencing free surface flow conditions) with a width of several times the grain sizes build on the hydraulic control principle. This sub-type of check dams has been applied for more than a century (Piton et al., 2017). Colar (1970), and Armanini et al. (1991) provide a review on slit dams and design criteria for intentional self-flushing (see also Armanini & Larcher, 2001; Ferro, 2013).

So far, most flow control structures have been designed as either mechanical or as hydraulic control structures only. The combination of both controls was introduced in a recent research project (Schwindt, 2017). The sediment trap design from Schwindt (2017) aims at the reliable trapping of desired sediment volumes during hazardous bed-load-laden floods. In theory, the concept simultaneously enables sediment transport continuity during non-hazardous floods to prevent downstream sediment starvation and high dredging costs (an advantage of hydraulic control structures) while preventing self-flushing (the advantage of mechanical control structures). The main elements are shown in (Fig. 1(a)). These include a guiding channel in the deposition basin, which determines the wetted cross-section, and therefore, the flow conditions upstream of a *hybrid* flow control structure (referred to as *barrier* in the following). The guiding channel enables the passage of sediment across the deposition basin up to its bankfull discharge. The latter should be chosen depending on the lowest bedload transport capacity of downstream artificial (for example a bridge) or morphological bottlenecks when flooding occurs (see also later discussion in this paper). The deposition is initiated by a hybrid mechanical-hydraulic control barrier, which consists of an open check dam with a bottom orifice and an upstream bar screen with a bottom clearance (Fig. 1(b)). Both the guiding channel and hybrid barrier were systematically tested by Schwindt et al. (2018) in a laboratory flume showing promising results, but only with a single dam height and sediment mixture. These experiments proved the interest of hybrid structures compared to slits, slots, or rack check dams.

Even though the concept for permeable sediment traps (presented in Schwindt et al., 2018) builds on exhaustive flume experiments, four fundamental issues remain open until now: (1) Schwindt (2017) ran experiments with relatively coarse sediment and grain size sensitivity (variability) was not studied. (2) Schwindt (2017) only used a single control structure height to impose backwater that drives hydraulic control, where the possible effect of higher barrier heights is still unknown. (3) The occurrence of driftwood was not tested with the argument that wood does not occur during small flood events. However, wood may always be present in mountain rivers and additional tests were required. (4) Schwindt (2017) used a case study to establish the combined (*hybrid*) control principle, but validation with other data was missing.
To resolve these open research issues, the current study uses a new systematic test series on the modified flume from Schwindt (2017) as well as an independent case study of a mountain river in

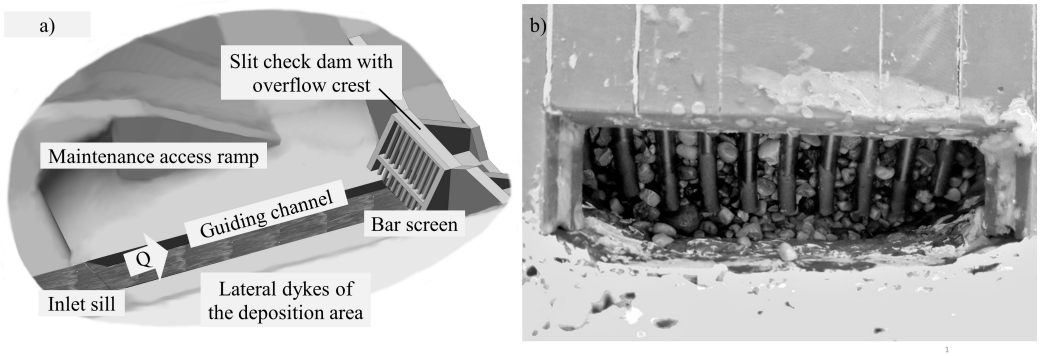

Fig. 1. a) Structural elements of a permeable sediment trap (adapted from Schwindt (2017)). The barrier consists of an open slit check dam for hydraulic control and an upstream bar screen for mechanical control. The overflow crest serves for flood discharge evacuation. The hydraulic conditions upstream of the barrier are governed by a guiding channel across the deposition area. b) View of the hybrid barrier from downstream. The bar screen with bottom clearance is visible through the opening of the slit check dam.

the French Alps. In the flume experiments, a finer sediment mixture is used to assess grain size sensitivity and improve design recommendations for the bar screen. Moreover, the influence of the barrier height is systematically tested to analyze the relation between backwater depth, grain size, and self-flushing. Thus, a new dimension of complexity is introduced, which has to be considered in the design of flow control structures in practice. With the case study of the mountain river Combe de Lancey in the French Alps (Piton et al., 2019), additional study of complex interactions between sediment deposition and large wood retention under variable sediment supply conditions (characteristic for mountain rivers, as reported in Rainato et al., 2016) is done. Eventually, the case study enables development of a design appendix for the permeable sediment trap from Schwindt et al. (2018) to account for wood, which may trigger typical failure mechanisms of flow control structures (see failure mechanisms reported in Bezzola et al., 2004). Therefore, in this paper the four open issues from Schwindt (2017) are answered through novel insight from systematic experimental campaigns in a generic laboratory flume and a case study. The new experimental campaign results in new practice-oriented recommendations, which are thoroughly discussed.

This paper starts with a description of the two experimental set ups (generic flume and case study), the test procedures and the dimensionless parameters used in the analysis. Second, new experimental results on the influence of bar screen features (bottom clearance height and space between bars) and barrier height, as well as the behavior of the hybrid barrier with a generic hydrograph are presented. The systematic experiments investigate conditions when hybrid barriers may perform better than pure hydraulic control structures to avoid possible undesired self-flushing. Finally, gravel and large wood transport are discussed for the case study (small-scale physical model) of the Combe de Lancey creek. The discussion also features the uncertainty involved in design parameters and structural adjustments, as well as recommendations on using either single slot (hydraulic control) or hybrid barriers.

2. Methodology

2.1. Experimental set up

The current paper presents two independent experimental campaigns. The first campaign consists of a systematic parameter study performed at the laboratory of hydraulic constructions (LCH) of Swiss Federal Institute of Technology Lausanne (EPFL, Switzerland), where systematic, parametric experiments were carried out on an established experimental set up based on Schwindt et al. (2018). The second campaign consists of a case study of a French creek done at the Artelia laboratory in Grenoble (France). The case study of the Combe de Lancey creek in the French Alps supports the discussion and refines the findings from the systematic experiments.

2.1.1. The generic set up for systematic experiments at LCH

To represent typical relations among channel width, grain size, discharge, and flow depth, the generic experimental set up at LCH was built based on the geometric dimensions of 132 characteristic data sets from mountain rivers collected by Schwindt et al. (2018). Thus, the set up does not represent a specific prototype configuration, but rather a generic average of multiple mountain rivers with channel slopes in the range of 0.02-0.06 m/m. Considering Froude and Shields similitude, the applicable geometric scale is between λ = 1:10 - 1:40.

Previous tests done by Schwindt et al. (2018) used a relatively coarse grain size mixture with D_{84} = 13.7 mm and D_{95} = 17.4 mm (the latter approximately corresponds to 17 cm - 70 cm in the field using a scaling of $\lambda = 1:10 - 1:40$). D_{i} is the diameter for which i percent of the sediment particles are finer. The finer sediment mixture used in the current study had the following characteristics: D_{30} = 5.6 mm; D_{50} = 6.4 mm; D_{84} = 8.0 mm; D_{95} = 9.4 mm; D_{100} = 16 mm; and σ = 1.26, where $\sigma = 0.5\,(D_{84}/D_{50} + D_{50}/D_{16})$. The here used D_{95} corresponds to approximately 9 cm - 38 cm at $\lambda = 1:10 - 1:40$.

A fixed, rough channel bed was used in the experiments. Therefore, the transported sediment does not originate from the bed. However, the sediment transport mode was bedload-like, which enables the comparison of the experimental sediment transport with mountain river bedload. The laboratory flume had a 2.5-m-long adaptation reach for sediment and water mixing upstream of a 3-m-long observation reach (Fig. 2). The sediment was stored in a cylindrical container with a bottom screw to control the supply rate. The sediment was wetted before every experiment to ensure similar initial conditions. Subsequently, the sediment was released onto a system of conveyor belts that delivered the sediment to the adaptation reach, along with the water from the laboratory pump system. The pump discharge was registered every three seconds by an electromagnetic flow meter (type ABB FXE4000) with a precision of 0.1%.

The wet outflowing sediment was captured in a sieve at the downstream end of the model. After one minute the sieve was weighed. For practical reasons, only one weight measurement every two minutes could be done with a scale that had a precision of ± 2 g (type Kern 440 51N). In addition, the total weight of the collected sediment was measured at the end of every experiment using a wireless industrial scale (type Dynafor MWXL-5, with a precision of ± 0.01 kg) attached to the filter basket. The sediment that remained in the experimental set up at the end of every experiment was flushed and also weighed with the industrial scale. The deposition pattern was recorded using a top-view camera (GoPro Hero Silver, 2016) that recorded a picture every 10 s. Additionally, the extent of the final deposit was recorded using a motion sensing camera (Microsoft Kinect V2).

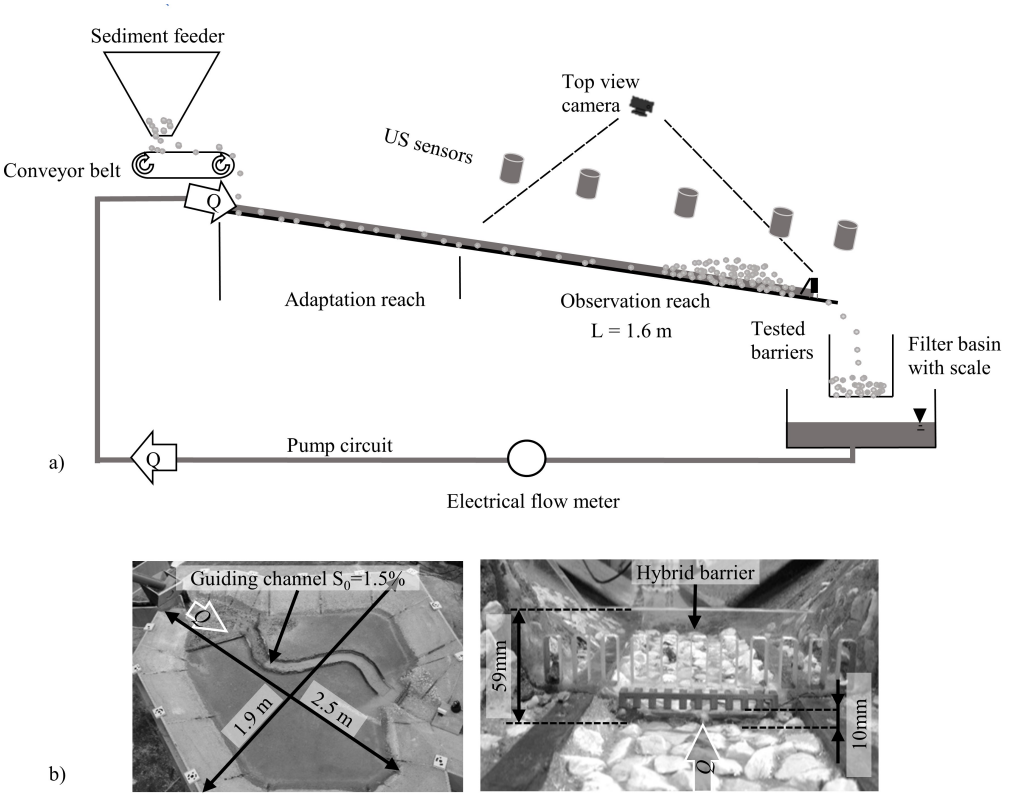

Fig. 2. a) Sketch of the set up for the generic model experiments at LCH. Sediment and pump discharge were supplied at the top of the adaptation reach. After mixing by transportation, the sediment-water mixture entered the observation reach. The water depth was measured by ultrasound (US) - sensors. Sediment was either retained by the barrier in the deposition area or captured in a filter basket at the downstream end of the set up. b) Set up of Artelia's scaled model study for Combe de Lancey creek (top view of the whole model (left) and upstream view of the barrier (right)).

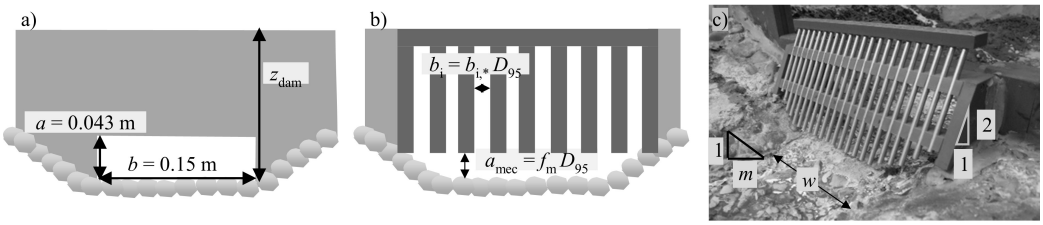

Fig. 3. a) Parameters of the hydraulic barrier (slot orifice). b) Parameters of the mechanical barrier (bar screen). c) Picture of the generic experimental set up with a bar screen installed and the parameters of the guiding channel. In the hybrid barrier set up, the bar screen is placed upstream of the slot check dam (Fig. 1(b)).

The observation reach of the sediment trap consisted of a deposition basin with a guiding channel and downstream barrier. The deposition area had a width of 1.20 m and a length of 1.60 m. The guiding channel had a bankfull discharge of Q_{bf} = 5.5 l/s, which corresponds to the target discharge up to which no retention was desired. The flow depth at Q_{bf} was approximately 0.032 m. The guiding channel had a bottom slope of S_0 = 6% and a bottom width of w = 0.11 m (see Fig. 3). Its bank inclination was m = 2.25 and the fixed channel bed was paved with pebbles larger than the D_{84} of the transported sediment. According to the analysis done by Schwindt (2017), the discharge-dependent roughness of the channel corresponded to a Manning's n of approximately 0.02. A check dam-like barrier with a slot orifice served as a hydraulic sediment transport control device (Fig. 3). The geometry of the slot orifice with a height of a = 0.043 m and width of b = 0.15 m was chosen according to Schwindt (2017) to enable sediment passage up to the target discharge for retention, Q_{bf}. The barrier height, z_{dam}, was varied during the experiments. For evaluating mechanical control with finer sediment, a bar screen was placed upstream of the open check dam as a mechanical control with an inclination of 2:1 to favor the passage of driftwood over the crest (D'Agostino et al., 2000; Piton & Recking, 2016b). The bar screen's bottom clearance height, a_{mec} and the spacing between the bars b_i were varied during the experiments. More details on the experimental set up can be found in Roth (2017).

2.1.2. Combe de Lancey case study set up at Artelia's laboratory

The physical model of the French creek Combe de Lancey had a geometric scale of λ = 1:40, respecting Froude and Shields similitude. The sediment deposition basin was considerably larger than the basin used in the generic experimental set up, being approximately 2.5 m wide and long (100 m at prototype scale, which is given in the following between parentheses), with a diamond planar shape (Fig. 2(b)). It had a bottom gradient of 1.5% and was equipped with a 13-mm deep (0.5 m) and 88-mm large (3.5 m) guiding channel that precisely represents the flow capacity of Q_{bf} = 0.7 l/s (7 m^3/s) at a downstream bottleneck (see discussion in Section 5). A hybrid barrier was placed at the basin outlet. The structure had a 13-mm high (0.5 m) and 100-mm wide (4 m) slot orifice (see Fig. 2b and Fig. 11). The bar screen had a clearance height of 10 mm (0.4 m) and a spacing between the bars of 5 mm (0.2 m). This corresponds to a bar spacing of 0.6 - 0.74 D_{95} and a clearance height of 1.2 - 1.5 D_{95}. The range corresponds to the two grain size distributions that were tested to validate the robustness of the structure (see later). The spillway (barrier crest) was set to set at 58.7 mm (2.35 m), which is higher than the bar screen, because the determining

factor for the barrier height was the target trapping volume of 0.315 m^3 (20,000 m^3). In contrast to the generic experimental set up at LCH that had a smaller basin, the target volume of the case study was calculated considering a deposition slope of 4%. Eleven vertical slots, 10-mm (0.4 m) wide and 25-mm (1.0 m) high, were cut into the structure between the spillway and the top of the bar screen. The vertical slots were expected to be obstructed by large wood and coarse grains as was the bar screen in the case of floods higher than Q_{bf}. They were added to enable a continuous flow downstream. Even when the bottom bar screen is jammed, flows will not be transiently stopped with sudden dam surge flow when the dam is overtopped. The spillway corresponded to a trapezoidal weir with a 150-mm (6 m) wide base, 45° side slopes and a height that should be enhanced and specified with the small-scale modeling (Fig. 11(d)).

2.2. Experimental procedures

The driving parameters of the hybrid barrier were the following: (i) the barrier's total height, (ii) the bar screen's bottom clearance height, (iii) the bar spacing, (iv) the orifice bottom elevation, and (v) the orifice bottom width. The two latter were thoroughly studied by Schwindt et al. (2017). The three first are systematically investigated in the current study.

First, steady-state tests were done to verify and adjust, if necessary, the bar screen parameters (bar spacing, clearance height). In a second stage, hydro-morphodynamic experiments (i.e., with a flood hydrograph with sediment injections) were done to analyze the barrier height effect on the occurrence of self-flushing. The hydro-morphodynamic experiments also served for testing the vulnerability of the hybrid barrier concept. In these vulnerability experiments, one bar screen design (bar spacing and clearance height) was used that corresponded exactly to the design requirements as a multiple of the finer characteristic grain sizes used in this study and another bar screen design was used that corresponded to the multiple of the coarser sediment mixture used in Schwindt et al. (2017). However, the finer grain size mixture was always used even though the coarse structure was not designed for it. Thus, testing was aimed at the vulnerability of the hybrid barrier when the actually present sediment is finer than expected during the design of the bar screen.

2.2.1. Study of mechanical deposition control

The bedload transport capacity, $Q_{b,max}$, which describes the maximum sediment supply rate that does not cause deposition in a flume for a given discharge, was first evaluated for the non-constricted guiding channel to obtain reference values (denoted as $Q_{b,max,1}$ in the following). Subsequently, the reduced bedload transport capacity $Q_{b,max,j}$ was evaluated with variable bar spacing and clearance height of the bar screen. The bar screen configurations were tested with steady discharges ranging from 3.5 l/s to 7.2 l/s, which correspond to discharges that are slightly lower and higher than the guiding channel's flow capacity (Q_{bf} = 5.5 l/s). Each discharge was tested with increasing sediment supply, in order to accurately determine the bedload transport capacity for a given discharge. The experiments are summarized in Table 1. Because of the presence of the bar screen, the bedload transport capacity did not increase with discharge as would have been the case in a non-constricted channel. Here, the bedload transport capacity reached a peak and subsequently the bar screen progressively clogged and retained increasingly more sediment. The experimental results indicate the discharge-dependent bedload transport capacity of any given bar screen set up. The objective here was to determine the relevant bottom clearance height to strongly decrease sediment transport when $Q > Q_{bf}$ while marginally changing sediment transport when $Q < Q_{bf}$.

Table 1. Experiments for assessing the bedload transport capacity of a guiding channel and bar screen with bottom clearance. N is the number of experiments for every relative bar spacing $b_i, * = b_i/D_{95}$ tested with varying relative bar screen bottom clearance height $f_m = a_{\mathrm{mec}}/D_{95}$ and varying steady discharges Q. Q_{min} and Q_{max} represent the range of tested discharges.

$b_{\mathrm{i},*}$ [-]	f_{m} [-]		Q [l/s]		N
	$f_{\mathrm{m,min}}$	$f_{\mathrm{m,max}}$	Q_{min}	Q_{max}	
0.57	1.25	2.55	3.0	5.5	117
0.94	1.37	1.49	3.0	5.5	38
1.04	1.70	1.70	4.0	5.0	9
1.15	1.36	1.69	3.0	7.0	61
					$\sum = 225$

2.2.2. Study of pure hydraulic deposition control

The hydraulic deposition control was tested using a generic hydrograph to simulate a flood event with possible self-flushing. It is worth stressing that no bar screen was added to the slit check dam during these experiments. The hydrograph shape was based on Schwindt et al. (2017) and had the following characteristics:

- Duration of the falling limb $t_- = 1.7$ times the duration of the rising limb $t_+ = 1129\,\mathrm{s} \approx 19\,\mathrm{min}$, which is characteristic for floods in mountain rivers in the range of the applicable scales, and used in several other, similar experiments (Armanini & Larcher, 2001; Piton et al., 2018b; Schwindt et al., 2018).
- The initial discharge equals the bankfull discharge of the guiding channel ($Q_{\mathrm{bf}} = 5.5$ l/s) and the peak discharge was limited by model constraints ($Q_{\mathrm{max}} = 12.5$ l/s). The discharge was increased in steps of 4 minutes to generate quasi-unsteady conditions.
- The ratio of the sediment supply rate $Q_{\mathrm{b,i}}$ and the discharge Q was 0.5% (weight-specific) for each step.

The dimensionless hydrograph with sediment supply is shown in Fig. 4.

The trapping efficiency of the barrier was recorded using a camera and quantified through the sediment volume retained upstream of the barrier, V_{dep}. Seven barrier heights ranging from 0.11 to 0.152 m were tested, with constant orifice dimensions as listed in Table 2.

2.2.3. Study of the hybrid barrier

The hybrid barrier was tested with the same generic hydrograph used in the experimental campaign for the pure hydraulic deposition control. Every configuration was tested twice to verify that the observations made can be confirmed and are replicable. An exploratory test of vulnerability was done using a bar screen originally designed for coarser sediment, to verify if it would clog also with finer sediment. The experiments are summarized in Table 3.

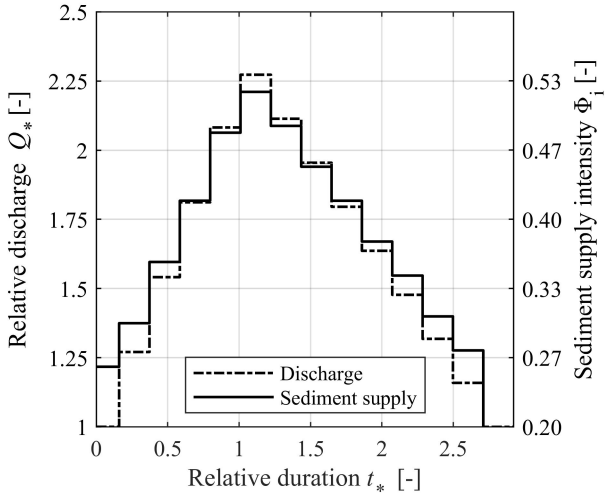

Fig. 4. Generic hydrograph of an experimental flood event. The relative discharge $Q_* = Q/Q_{\mathrm{bf}}$ (left vertical axis) and the sediment supply intensity $\Phi_{\mathrm{i}} = Q_{\mathrm{b,in}}/(w\ \rho_{\mathrm{f}}\sqrt{(s-1)\ g\ D_{84}^3})$ (right vertical axis) are shown as a function of the relative hydrograph duration $t_* = t/t_+$. Here t_+ denotes the duration of the rising limb, ρ_{f} =the water density, s = specific gravity of the sediment, and g = gravitational acceleration.

Table 2. Experiments for evaluating pure hydraulic deposition control. Most configurations were repeated twice with α indicating the first and β indicating the second run. $V_{\Sigma*} = V_{dep}/V_{trap}$ is the relative supply volume after a hydrograph where V_{trap} is the trap capacity and V_{dep} is the volume of the sediment deposit. V_{supply} is the total supplied volume during a hydrograph, and z_{dam} is the barrier height.

z_{dam} [m]	Run	V_{trap} [m^3]	V_{supply} [m^3]	$V_{\Sigma*}$ [-]
0.122	α	0.149	0.10	Abandoned after peak
0.122	β	0.149	0.09	Abandoned after peak
0.124	α	0.154	0.20	1.30
0.124	β	0.154	0.20	1.31
0.126	α	0.159	0.20	1.27
0.132	α	0.174	0.20	1.16
0.132	β	0.174	0.21	1.19
0.142	α	0.202	0.20	1.01
0.142	β	0.202	0.20	1.01
0.148	α	0.219	0.20	0.93
0.148	β	0.219	0.21	0.95
0.152	α	0.231	0.21	0.92
Total number of experiments			12	

Table 3. Conducted experiments for the hybrid barrier. With relative bar spacing $b_{i,*} = b_i/D_{95}$, relative bar screen bottom clearance height $f_m = a_{mec}/D_{95}$, and relative supply volume $V_{\Sigma,*} = V_{supply}/V_{trap}$.

Bar screen		Slot check dam				
$b_{i,*}$ [-]	f_m [-]	z_{dam}[m]	V_{trap}[m^3]	V_{supply}[m^3]	$V_{\Sigma*}$[-]	Run
1.15	1.57	0.11	0.121	0.19	1.57	α,β
1.34	2.55	0.11	0.121	0.22	1.81	α

2.2.4. Case study

The grain size of the sediment transport during extreme events is uncertain. Based on field measurements and a historical analysis, it has been considered that D_{95} is in the range of 0.27 to 0.33 m. The flood duration and solid matter concentration are also uncertain. Several runs with 0.315 m^3 (20,000 m^3 of cumulative bedload transport at prototype scale) thus, were tested with different hydrograph durations of 2.2 (14), 2.8 (18) and 4.7 h (30 h) and peak discharges of 2.2 (22) and 3.5 l/s (35 m^3/s), for 30- and 100-year flood return periods, respectively. The geomorphic scenarios that led to the definition of these boundary conditions are described in Piton et al. (2019). Both field survey and historical data indicated that large wood pieces can be mobilized for flows higher than the bankfull discharge. A volume equivalent to 1.6 l (100 m^3) of large wood was systematically and evenly introduced during the hydrograph's rising limb when the discharge passed 1.5 l/s (15 m^3/s) (i.e., a 10-year return period). More frequent events were assumed to regularly flush wood. Thus, marginal wood supply was assumed for low flows while the recruitment of such a large volume seems likely during events of higher magnitude; for example, volumes of 600 m^3 were mobilized in a 2005 post-flood survey.

2.3. Dimensionless parameters

2.3.1. Background

A detailed dimensional analysis was done by Schwindt (2017) for a similar experimental set up, where the processes analyzed and the parameters involved were identical to the ones in the current study. Therefore, the dimensionless parameters used for the current analysis are introduced in this section by referring to the dimensional analysis in Schwindt (2017) (based on D'Agostino, 2013; Einstein, 1950; Yalin, 1977). Thus, the scaling of the here considered hydro-morphodynamically governed processes is based on the similitude of the Froude number and Shields number in the experiments and prototype applications.

2.3.2. Mechanical control

For sediment transport related, hydrodynamic phenomena, D_{84} is considered the governing characteristic grain size (MacKenzie et al., 2018; Piton et al., 2017). However, for mechanical blockage the governing grain size is D_{95}, consistent with recommendations of previous studies on the clogging of open check dams made of steel frames (D'Agostino, 2013; Ikeya, 1989; Itoh et al., 2011, 2013; Yuan et al., 2019; Watanabe et al., 1980). In addition, Shima et al. (2016) investigated the size of grains leading to the clogging in the field and these authors concluded that the D_{95} was the relevant size. With the differentiation of using D_{84} for hydrodynamic process descriptions and D_{95} for mechanical blockage, the gap between previous research dedicated to hybrid barriers (using strictly D_{84}) and past research dedicated to debris flow and bedload trapping with steel structures is bridged. Thus, the following parameters were used in the analysis of the experimental results:

- $f_m = a_{mec}/D_{95}$, relative bar screen bottom clearance height;
- $b_{i,*} = b_i/D_{95}$, relative bar spacing;
- $Q_* = Q/Q_{bf}$, relative water discharge;
- $\theta = Q_{b,max,j}/Q_{b,max,1}$, normalized sediment transport.

where a_{mec} denotes the clearance height below the bar screen, Q is the discharge and Q_{bf} = 5.5 l/s the bank full discharge of the guiding channel, which corresponds to the target discharge for retention. $Q_{\mathrm{b,max,1}}$ and $Q_{\mathrm{b,max,j}}$ are the bedload transport capacity of the non-constricted and constricted channel, respectively.

2.3.3. Hydraulic control

In line with the foregoing reasoning, g, ρ_{f}, and D_{84} are considered as set of independent variables. Flow depth-related parameters are not considered here because of the rapidly varying shape of sediment deposits during the experiments that made accurate, non-intrusive measurements of the flow depth extremely complicated. The following set of dimensionless parameters underlies the analysis of the experimental results of hydraulic control structures and hydro-morphodynamic processes:

- $t_* = t/t_+$, relative duration of the hydrograph, where t_+ = 1129 s;
- $V_* = V_{\mathrm{dep}}/V_{\mathrm{supply}}$, relative deposit volume;
- $V_{\sum}* = V_{\mathrm{supply}}/V_{\mathrm{trap}}$, relative supply volume;
- $\Phi_{\mathrm{i}} = Q_{\mathrm{b,i}}/(w_{\mathrm{m}}\ \rho_{\mathrm{f}}\ \sqrt{(s-1)\ g\ D_{84}^3})$, sediment supply intensity, where $Q_{\mathrm{b,i}}$ is the sediment inflow;
- $\Phi_{\mathrm{o}} = Q_{\mathrm{b,o}}/(w_{\mathrm{m}}\ \rho_{\mathrm{f}}\ \sqrt{(s-1)\ g\ D_{84}^3})$, outflowing bedload intensity, where $Q_{\mathrm{b,o}}$ is the sediment outflow;
- $Fr = Q\ /\ \sqrt{g\ w_m^2\ h^3}$, Froude number, where h is the flow depth;

V_{dep} and V_{supply} are morphological parameters and denote the total volume of sediment deposited in the deposition area after an experimental run and the total supplied volume of sediment during an experiment, respectively. The trap volume capacity is imposed by the basin shape and slope, barrier height, and sediment deposition slope. In the experimental condition, the following equation provides a rough estimate for the trapping capacity:

$$V_{\mathrm{trap}} = \frac{w_{\mathrm{basin}} \cdot z_{\mathrm{dam}}^2}{2 \cdot S_0} \tag{1}$$

where w_{basin} designates the width of the basin, S_0 is the guiding channel slope, and z_{dam} is the barrier height. The equation neglects the deposition slope, which could be left out in the current experiments due to the relatively small basin sizes. Readers are invited to use alternative equations to estimate V_{trap} that may be more suitable for other case studies with different features.

Φ_{o} and Φ_{i} denote bedload supply and outflow intensity respectively (Einstein, 1950; Smart, 1984). $w_{\mathrm{m}} = w + m \times h_m$ denotes the mean flow width in the trapezoidal guiding channel with w the guiding channel bottom width and h_{m} the mean flow depth. The sediment specific gravity is defined as $s = \rho_{\mathrm{s}}/\rho_{\mathrm{f}}$ with ρ_{s} the sediment density and ρ_{f} the water density. The remaining parameters were previously defined.

3. Results

3.1. Mechanical control: Bar screen design parameters

3.1.1. Bar spacing

The experiments with mechanical control focused on discharge close to Q_{bf}. They were done only with a mechanical bar screen, without the orifice dam downstream. The observed normalized sediment transport, $\theta = Q_{b,max,j}/Q_{b,max,1}$, is shown in Fig. 5 as a function of the dimensionless discharge, $Q_* = Q / Q_{bf}$, for all tested bar screen configurations. Such barriers should optimally enable sediment passage for events with discharges up to the bankfull discharge of the guiding channel ($Q_* = 1$) and trap sediment for higher discharges. The desired barrier permeability at smaller discharges $Q_* < 1$ is indicated by large values of the normalized sediment transport $\theta = 0.75$ to 1 (i.e., little to no reduction of transported sediment compared to a guiding channel without a bar screen). Reduced values of θ for $Q_* > 1$ compared to discharges $Q_* < 1$ indicate a reduction of the transport capacity with a high clogging probability (very fast clogging), and, therefore, reliable retention of larger, potentially hazardous sediment transport.

Irrespective of the clearance height and discharge, large reductions of the normalized sediment transport ($\theta < 0.2 - 0.4$) were observed for a relative bar spacing $b_{i,*} \leq 0.94$. This is the case for all tested configurations except for $b_{i,*} = 0.57$ with a relative clearance height of $f_m = 2.55$ and $Q_* < 0.7$. In this special case, the water surface did not touch the bar screen, and, thus, did not disturb sediment transport.

Fig. 5 shows that a relative bar spacing of $b_{i,*} = 1.04$ and $b_{i,*} = 1.15$ reduces θ to approximately 0.75 for $Q_* < 1.0$ with large amounts of sediment passing the barrier without interruption. For $Q_* > 1.0$, θ is reduced to approximately 0.6, depending on the clearance height of the bar screen. Bar spacing $b_{i,*} \geq 1.04$ fulfills the requirements for safe retention at $Q_* > 1.0$ and barrier permeability for $Q_* < 1.0$. For non-hazardous discharges ($Q_* \leq 1$), a maximum permeability of the barrier is desirable. Therefore the largest relative bar spacing providing reliable retention for $Q_* > 1.0$, namely $b_i = 1.15$ was retained for the further analysis.

3.1.2. Bottom clearance height

To determine a suitable relative bar screen bottom clearance height, $f_m = a_{mec}/D_{95}$, several screen configurations with the afore mentioned optimal relative bar spacing of $b_{i,*} = 1.15$ are compared. As can be seen in Fig. 6, which represents a magnification of part of Fig. 5, a relative bottom clearance height of $f_m = 1.68$ results in large values of $\theta \approx 0.75$ (i.e., high relative sediment transport), independent of the discharge. Furthermore, for this clearance height, the bedload transport capacity was not limited by bar screen clogging, but by deposition in the channel upstream and downstream of the barrier, which implies that the bar screen did not have the desired effect. For bar screens with a relative bottom clearance height of $f_m = 1.36$ - 1.57, the bedload transport capacity was governed by quickly entangling grains with increasing sediment supply. However, a relative bottom clearance height of $f_m = 1.36$ led to low values of the normalized sediment transport $\theta = 0.54$ also for nonhazardous discharges ($Q_* = 0.95$). Therefore, the small clearance height did not provide the desired permeability. The maximum relative bottom clearance providing reliable retention for high discharges, while maximizing barrier permeability at small discharges, corresponds to $f_m = 1.57$.

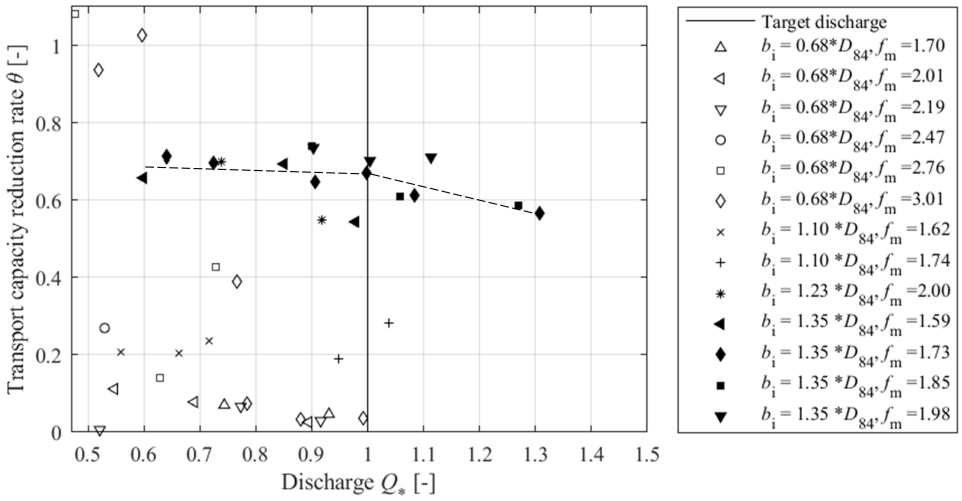

Fig. 5. Normalized sediment transport, $\theta = Q_{b,max,j}/Q_{b,max,1}$, as a function of the relative discharge, $Q_* = Q/Q_{bf}$, for all tested bar screen configurations. For non-hazardous discharges (i.e., $Q_* < 1$), $\theta > 0.75$ indicates favorable sediment permeability of the barrier. For hazardous discharges (i.e., $Q_* > 1$), a reduction in the sediment transport capacity θ compared to $Q_* < 1$ is desirable. The dotted line qualitatively indicates the trend for a relative bar spacing of $b_{i,*} = 1.15$.

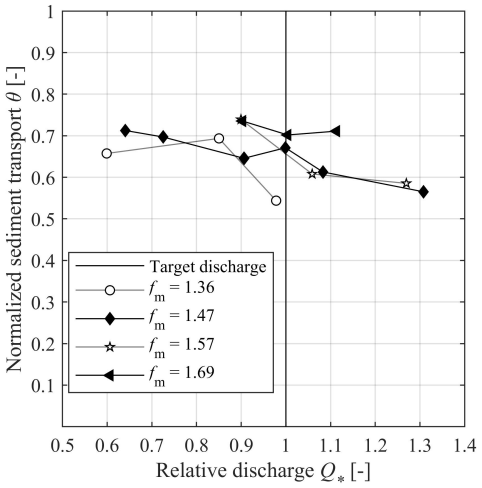

Fig. 6. Normalized sediment transport, $\theta = Q_{b,max,j}/Q_{b,max,1}$, as a function of the relative discharge, $Q_* = Q/Q_{bf}$, for $b_{i,*} = 1.15$ with variable bottom clearance height, f_m, of the bar screen configurations tested.

3.2. Pure hydraulic control: Required trap capacity to prevent undesired self-flushing

The experiments with hydraulic control were done without a bar screen, only with the slot check dam-like barrier. Fig. 7 shows the sediment outflow pattern for different relative supply volumes, $V_{\Sigma*} = V_{\text{supply}}/V_{\text{trap}}$, as a function of the relative hydrograph duration, t_*. Repetitive runs with the same barrier, α and β, confirm that the experimental results are reproducible. For reasons of readability, not all runs are plotted. The complete data are listed in Table 4. The sediment retention was initiated at $t_* = 0.16$ in all test runs, which is represented by a strong reduction in the outflowing bedload intensity, Φ_o. The hydraulic deposition initiation corresponds to the increase in the discharge to $Q_* = 1.27$ when the free surface flow capacity of the orifice is exceeded. The sediment deposit subsequently grew in the upstream direction, with layer-wise filling of the guiding channel.

For relative supply volumes larger than $V_{\Sigma*} = 1.3$, the outflow never reached zero and most of the previously deposited sediment was flushed at $t_* \approx 0.7$. Flushing occurred before the peak and led to a temporary sediment outflow larger than the sediment inflow. After the flushing, no new deposition occurred and the sediment outflow corresponded approximately to the inflow. For $V_{\Sigma*} > 1.3$, less than 20% of the supplied sediment volume remained in the deposition area at the end of the test runs, but the amount increased with increasing barrier height and trap volume (decreasing $V_{\Sigma*}$). The deposition pattern at the peak ($t_* = 1$) is shown in Fig. 8a. The shown deposition has a horseshoe shape due to material being flushed. Deposits remained only on both sides of the guiding channel and directly upstream of the barrier. The deposits on the sides indicate the maximum extent of the deposited material before flushing.

The amount of sediment that was flushed decreased with the relative supply volume approaching one. An increasingly large deposit directly upstream of the barrier is not flushed, which leads to an increase in the relative retained volume at the end of the experiment from $V_* = 0.07$ for $V_{\Sigma*} \approx 1.4$ to $V_* = 0.22$ for $V_{\Sigma*} \approx 1.16$ (see Fig. 9). The relatively small value of $V_* = 0.22$ for $V_{\Sigma*} \approx 1.16$ is due to partial self-flushing before the peak and an outflowing bedload intensity Φ_o at the peak similar to the inflowing bedload intensity.

As shown in Fig. 7, relative supply volumes of $V_{\Sigma*} = 1.01$-1.19 show a similar evolution of the outflowing bedload intensity, Φ_o, and both configurations retained approximately 22% of the total transported sediment. Sediment outflow intensities before the peak are below the sediment supply, resulting in a large deposit at the peak (Fig. 8(b)). The deposit shape was oval and much larger than the deposit for $V_{\Sigma*} \approx 1.4$ (Fig. 8(a)). Once the deposit height reached the height of the barrier, the deposit size remained stable, and the outflowing bedload intensity equaled the supplied sediment. No flushing was observed, but the peak outflowing bedload intensity was not reduced. Therefore, no reliable sediment retention is provided with the hydraulic control-only configuration if the volume of sediment supplied is significantly higher than the trap capacity.

The lowest tested relative supply volumes of $V_{\Sigma*} = 0.92$ to 0.95 had a different sediment outflow behavior compared to that with higher $V_{\Sigma*}$ (see Fig. 7). After the initial decline in sediment outflow, all supplied sediment was retained from $t_* = 0.4$ to $t_* = 0.58$. After the barrier had experienced overflow at $t_* = 0.58$, the outflowing bedload intensity increased but always stayed smaller than the sediment supply. After the peak, Φ_o quickly dropped to zero. This sediment outflow behavior is reflected in the large volume retained ($V_* \approx 0.6$). This is much larger than the volume retained in the tests with higher relative supply volumes, $V_{\Sigma*}$. However, between $V_{\Sigma*} = 0.93$ and 0.95 a high variability in sediment outflow and final relative retained volume is observed. The variability

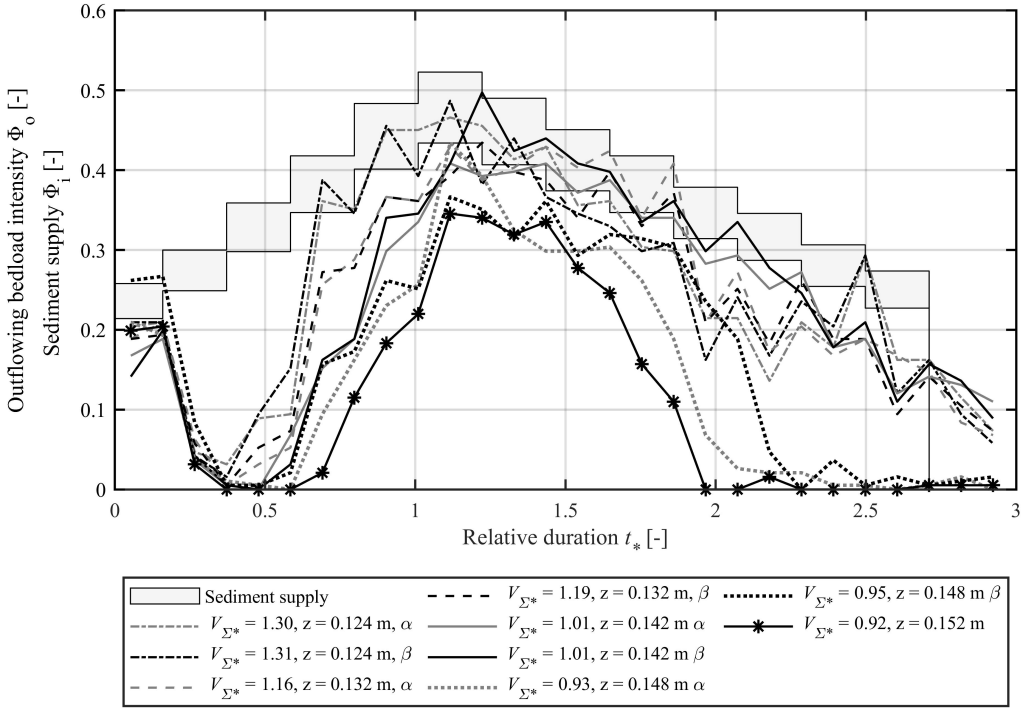

Fig. 7. Pure hydraulic control barrier: The outflowing bedload intensity, Φ_o, and the sediment supply intensity, Φ_i, as a function of the relative hydrograph duration, t_*, for the tested relative trap volumes, $V_{\Sigma*}$. For readability, some intermediate trap volumes are not plotted. The upper bound of the sediment supply is the target supply, and the lower bound is the target supply normalized with the minimum total volume that passed through the experimental set up during a hydrograph experiment. $\Phi_o \geq \Phi_i$ indicates self-flushing or a barrier that is literally transparent for sediment transport.

Table 4. The outflowing bedload intensity, Φ_o[-], during the hydrograph for all tested trap volumes V_{trap}.

z_{dam}	[m]	0.122	0.122	0.124	0.124	0.126	0.132	0.132	0.142	0.142	0.148	0.148	0.152
V_{trap}	[m^3]	0.149	0.149	0.154	0.154	0.159	0.174	0.174	0.202	0.202	0.219	0.219	0.231
V_{supply}	[m^3]	0.10	0.09	0.20	0.20	0.20	0.20	0.21	0.20	0.20	0.20	0.21	0.21
$V_{\Sigma*}$	[-]			1.30	1.31	1.27	1.16	1.19	1.01	1.01	0.93	0.95	0.92
Run		α	β	α	β	α	α	β	α	β	α	β	α
Q_*	t_*	Φ_o	Φ_o	Φ_o	Φ_o	Φ_o	Φ_o	Φ_o	Φ_o	Φ_o	Φ_o	Φ_o	Φ_o
1.00	0.05	0.20	0.19	0.20	0.21	0.19	0.19	0.19	0.17	0.14	0.21	0.26	0.20
1.00	0.16	0.20	0.19	0.21	0.21	0.20	0.21	0.19	0.19	0.20	0.19	0.27	0.20
1.27	0.27	0.10	0.10	0.05	0.04	0.06	0.06	0.06	0.04	0.04	0.04	0.08	0.03
1.27	0.37	0.05	0.09	0.03	0.02	0.01	0.01	0.01	0.01	0.01	0.01	0.01	0.00
1.54	0.48	0.09	0.07	0.09	0.09	0.06	0.03	0.05	0.00	0.00	0.01	0.01	0.00
1.54	0.58	0.13	0.12	0.09	0.15	0.10	0.05	0.07	0.07	0.03	0.00	0.02	0.00
1.81	0.69	0.39	0.37	0.36	0.39	0.33	0.26	0.27	0.15	0.16	0.09	0.16	0.02
1.81	0.80	0.34	0.33	0.35	0.35	0.27	0.29	0.28	0.19	0.19	0.16	0.17	0.12
2.08	0.90	0.50	0.46	0.45	0.46	0.45	0.37	0.37	0.30	0.34	0.23	0.26	0.18
2.08	1.01	0.42	0.37	0.45	0.39	0.46	0.36	0.36	0.34	0.35	0.26	0.25	0.22
2.27	1.12	0.42	0.44	0.47	0.49	0.43	0.43	0.39	0.41	0.41	0.43	0.37	0.35
2.27	1.22	0.42	0.47	0.46	0.38	0.45	0.39	0.43	0.39	0.50	0.39	0.35	0.34
2.11	1.33			0.41	0.44	0.42	0.40	0.40	0.40	0.42	0.32	0.31	0.32
2.11	1.43			0.43	0.37	0.41	0.43	0.39	0.41	0.44	0.30	0.36	0.34
1.95	1.54			0.36	0.35	0.38	0.40	0.34	0.37	0.41	0.30	0.29	0.28
1.95	1.65			0.36	0.33	0.34	0.42	0.40	0.39	0.40	0.30	0.32	0.25
1.80	1.75			0.30	0.30	0.29	0.34	0.33	0.34	0.34	0.26	0.31	0.16
1.80	1.86			0.30	0.31	0.32	0.41	0.37	0.34	0.36	0.19	0.30	0.11
1.64	1.97			0.21	0.16	0.17	0.21	0.21	0.28	0.30	0.07	0.24	0.00
1.64	2.07			0.21	0.24	0.23	0.27	0.25	0.29	0.34	0.03	0.19	0.00
1.48	2.18			0.14	0.17	0.16	0.17	0.18	0.25	0.28	0.02	0.05	0.02
1.48	2.29			0.21	0.24	0.19	0.20	0.26	0.27	0.25	0.02	0.00	0.00
1.32	2.39			0.18	0.20	0.17	0.17	0.19	0.18	0.18	0.01	0.04	0.00
1.32	2.50			0.29	0.29	0.18	0.19	0.19	0.19	0.21	0.01	0.01	0.00
1.16	2.60			0.16	0.12	0.09	0.17	0.09	0.12	0.11	0.00	0.02	0.00
1.16	2.71			0.16	0.16	0.14	0.15	0.14	0.14	0.16	0.01	0.01	0.01
1.00	2.82			0.12	0.09	0.07	0.08	0.10	0.13	0.14	0.02	0.01	0.01
1.00	2.92			0.07	0.06	0.09	0.07	0.07	0.11	0.09	0.00	0.02	0.01

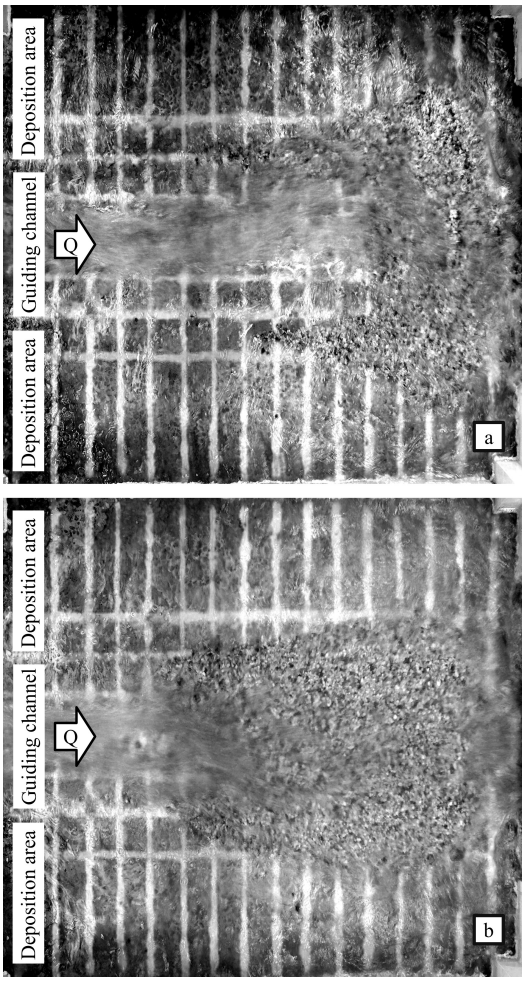

Fig. 8. Deposition pattern at the peak for different trap volumes: a) Flushing of the guiding channel with slight sediment deposits to both sides of the guiding channel at the peak discharge for $V_{\Sigma*} \approx 1.4$; and b) no flushing of previously deposited sediment for $V_{\Sigma*} = 1.01$. The shape of the barrier is visible at the right-hand edge of the images.

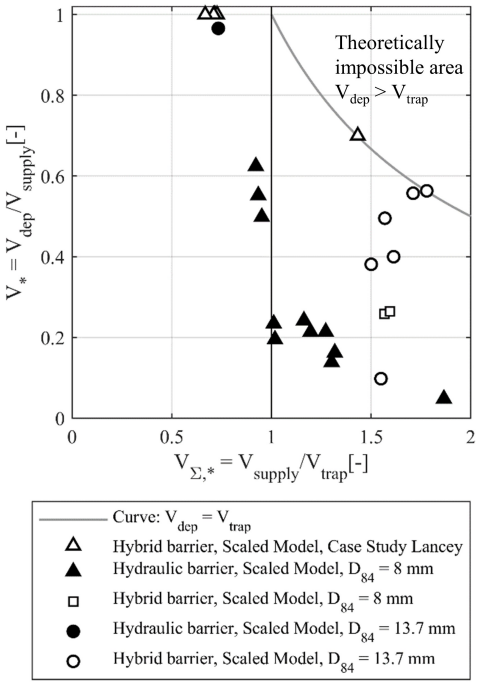

Fig. 9. Comparison of the relative deposited volume of sediments, V_*, for pure hydraulic (filled symbols) and hybrid barriers (empty symbols) based on three scaled models: (i) the generic model from this study (D_{95} = 9.4 mm), (ii) the case study Lancey (ARTELIA & IRSTEA (2018)) and (iii) Schwindt (2017) (D_{95} = 17.4 mm).

indicates that the behavior at approximately $V_{\Sigma*}$ = 0.94 is very sensitive to the relative supply volume, resulting in a large variability between the repetitive α and β runs. Reliable retention is only provided by relative supply volumes smaller than $V_{\Sigma*}$ = 0.92 (i.e., the supplied volume is slightly smaller than the trap capacity).

3.3. Study of hybrid barriers

Fig. 10 is similar to Fig. 7 for pure hydraulic barrier experiments. It shows the sediment outflow pattern for different relative supply volumes, $V_{\Sigma*} = V_{supply}/V_{trap}$, during the hydrograph for the hybrid barrier experiments.

If the bar screen is designed according to the recommendations found in the steady-state experiments, ($b_{i,*}$ = 1.15, f_m = 1.57), the bar screen clogs as soon as the target discharge for retention is exceeded at t_* = 0.2 (see Fig. 10). Subsequently, most of the transported sediment deposits ($\Phi_o << \Phi_i$) until the trap capacity is reached. The sediment outflow intensity increases again once the deposit height reaches the barrier height and subsequently becomes equal to the

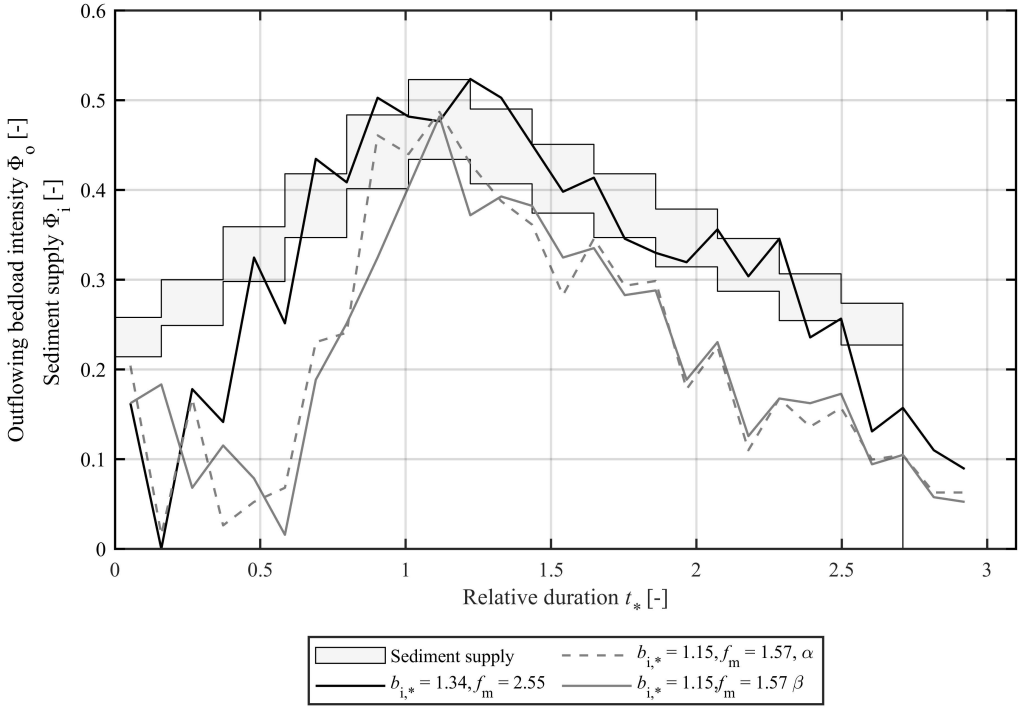

Fig. 10. Hybrid barrier: Outflowing bedload intensity, Φ_o, and the sediment supply intensity, Φ_i, as a function of the relative hydrograph duration, t_*, for the combined mechanical hydraulic deposition control. The plot shows the optimal design with a relative bar spacing of $b_{i,*} = 1.15$ and a relative bottom clearance height of $f_m = 1.57$ compared to a bar screen with $b_{i,*} = 1.34$ and $f_m = 2.55$ originally designed for coarser sediment. A very fast increase of Φ_o indicates self-flushing and $\Phi_o \geq \Phi_i$ indicates a barrier that is literally transparent for sediment transport.

sediment supply intensity. After the peak, some deposition is again initiated. Hence, the hybrid barriers differ from the pure hydraulic orifice-only barrier in that they do not self-flush and get more filled for similar supply conditions.

To validate the robustness and vulnerability of hybrid barriers regarding unexpectedly fine sediment supply, the possibility of clogging with a self-flushing sediment front was verified. A bar screen with specifications much larger than recommended ($b_{i,*} = 1.34$ and $f_m = 2.55$) and a large supply volume ($V_{\Sigma*} \approx 1.86$) was tested. For this mechanical bar screen without a superposed hydraulic barrier, no retention is expected.

In this case, sediment deposition is initiated by the hydraulic control barrier. As soon as the barrier experiences overflow at $t_* = 0.2$, all previously deposited sediment is flushed, and the bar screen is not clogged by the approaching self-flushing front (Φ_o increases rapidly until it becomes larger than Φ_i). Subsequently, no more sediment is retained ($\Phi_o = \Phi_i$). Thus, this bar design within the hybrid barrier acted as a pure hydraulic control barrier with too large $V_{\Sigma*} \approx 1.86$ and did not fulfill its retention function. This run demonstrated the importance of a suitable clogging of the bar screen.

4. Application example: The Combe de Lancey case study

The purpose of this section on the case study of the Combe de Lancey creek is to exemplify in a real case the reason why a hybrid barrier was chosen and to demonstrate its performance and robustness in the presence of large wood through a complementary experimental campaign. More details can be found in ARTELIA & IRSTEA (2018) and in Piton et al. (2019).

4.1. Description of the catchment basin

The 18 km^2 catchment of the Ruisseau de la Combe de Lancey creek is characterized by four main geomorphic units (Fig. 11(a,b)): (i) steep headwaters experiencing erratic debris flow activity; (ii) a 6 km-long, step-pool section in a 12%-steep mid-mountain range; (iii) 27%-steep bedrock and cascades gorges section; and (iv) a small alluvial fan that is fully occupied by the village of Villard-Bonnot. Here the channel is heavily constrained laterally and has an average slope of 1.5% from the fan down to the distal parts (Fig. 11(c)). The creek maximum discharge capacity of 7 m^3/s is determined where it passes on a canal bridge over a deep drainage ditch. Any additional discharge overflows the channel banks and is lost in the drainage ditch, and, thus, cannot help convey the sediment load down to the main river.

Long-lasting extreme rainfall on August 21 - 22, 2005, resulted in massive geomorphic adjustments in the stream and all neighboring catchments forming a flood event lasting for more than 24 h with peak discharges of moderate magnitude (close to 30-year return period peak discharges). Moreover, 20,000 m^3 of debris deposited at the main slope break of the fan (Fig. 11(b,c)) and plenty of large wood pieces were observed after the flood. Historic pictures showed that the only other catastrophic flood event occurred in 1939 with similar gravel and large wood deposits.

4.2. Why a hybrid structure at the Combe de Lancey creek?

A sediment bar situated at the confluence with the Isère River and dredging of sediment traps in neighboring catchments lead to the assumption that bedload transport occurs during annual high flows. The sediment transported by such annual events should not be trapped for environmental

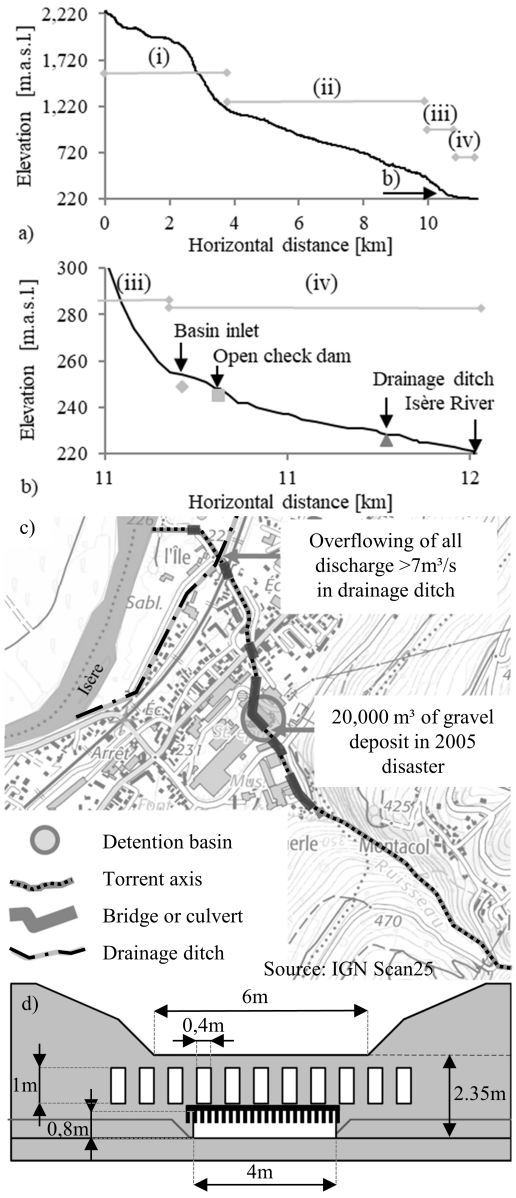

Fig. 11. a) Full longitudinal profile of the Combe de Lancey creek, divided into four sections (i) headwater, debris flow reaches, (ii) mid-range 12%-steep section, (iii) 27%-steep final gorges and (iv) alluvial fan; b) magnification of the fan section showing the location of the debris detention basin, drainage ditch, and confluence with the Isère River; c) map of the downstream gorge (iii) and alluvial fan (iv) sections as well as the location of bottleneck sections with deposition, jamming, and overflow issues; and d) open check dam upstream view: bottom slot equipped with an inclined bar screen.

reasons, to avoid unnecessary dredging, and to prevent channel incision across the village that could trigger undermining of the old stone walls protecting the banks or bridge abutments.
However, during high magnitude events as in the 2005 flood, if any geomorphic process, such as bank erosion or debris flow, supplies sediment to the torrent, the 12% slope of the catchment's mid-mountain range results in a very high sediment transport capacity. Field evidence showed that large wood pieces (1-4 m in length) and cobbles 0.3 to 0.5 m in diameter were available for transport in the gorge immediately upstream of the fan. These would be supplied in high numbers in the case of extreme events but cannot be transported through the whole fan channel. Therefore, they should be trapped upstream in a sediment trap. The slope knickpoint on the fan channel (Fig. 11(b)) and channel flow capacity limitations (7 m^3/s << 35 m^3/s, i.e., 100-year return period peak discharge) make the fan highly prone to sediment deposition. It is consequently necessary to enable sediment transport up to a discharge of 7 m^3/s but to trap and retain all gravel supplied at higher discharges. At the same time, the risk of self-flushing should be minimized. A hybrid structure was theoretically the best option to fulfill this objective and it was tested on a scaled physical model at the Artelia's hydraulic laboratory in Grenoble.

4.3. Proof of efficacy

For the sake of consistency with the previous sections, sizes are also given at prototype scale in this section (downscaling using Froude similitude enables model scale parameters to be computed). All runs followed similar geomorphic and hydraulic trajectories with to be various celerity and slightly random variations. In essence, the bedload transport was primarily observed in the guiding channel. Most of the sediment supply deposited near the basin inlet as soon as the discharge exceeded the 7 m^3/s threshold, as expected. The barrier orifice triggered a pressure flow for discharge Q < 7 m^3/s, thus, water depth significantly increased with discharge, even more when logs started clogging the upper slots. Moreover, the mild basin bottom slope enabled the entire basin to be rapidly flooded. The sediment deposit delta progressing upstream in the basin eventually reached the large wood jam at the end of these events (i.e., all sediment was trapped in the basin). Large wood was trapped near or at the barrier after transient deposition on sediment. As long as slots were freely flowing, logs were stuck against the structure by drag forces (e.g., Fig. 12(d)). In a second stage, for sufficiently high backwater, the flow velocity upstream of the barrier decreased below the aspiration threshold and a floating carpet formed (e.g., Fig. 12(a,e)).

Flows over the spillway occurred during every run but the floating carpet remained jammed at the spillway for the two events with peak flows of 22 m^3/s (Fig. 12(a-b)). Sudden releases of all floating logs were observed when the discharge approached 34 m^3/s for events with peak discharges of 35 m^3/s (Fig. 12(c-f)). In these cases, only the logs stuck at the barrier remained, but the floating carpet was released downstream. However, the sediment remained completely trapped in the basin because the opening was obstructed by a mixture of cobbles and the remaining logs. In essence, the hybrid structure was primarily jammed by large wood and secondarily jammed by sediment, as expected.

Some exploratory tests were done to investigate if the design would also work in the total absence of wood. All wood logs were manually removed. The discharge was restored, and the hybrid structure and upper slots were rapidly jammed by coarse grains. The structure was, thus, considered robust to fulfill its main function: sediment trapping for events higher than the frequent, routine events (< 7 m^3/s) and up to the design event (20,000 m^3 of gravel, peak discharge 22-35 m^3/s), with or without large wood.

Fig. 12. Interactions of the hybrid structure with large wood: (a) a large wood jam fully formed with a floating carpet forming upstream of the structure; (b) the end of the nonreleasing experiment, clear sorting of the large wood jam stuck against the structure and sediment filling the basin upstream cab be seen. The steps of release processes are constituted by (c) the beginning, where the barrier is free of wood and the flow is confined by the guiding channel; (d) wood becomes stuck at the barrier and partially obstructs the slots; (e) the fully formed large wood jam with an upstream floating carpet, and (f) a few seconds later, when the large wood floating carpet is released downstream and single logs remain stuck at the barrier (picture courtesy of Artelia and Villard-Bonnot municipality).

A safety check event that was tested with a twofold sediment volume demonstrated that the maximum sediment retention capacity without freeboard was 37,000 m^3, while the remaining 13,000 m^3 overtopped the barrier crest when the basin was completely filled. The trapping efficiency and supply up to the capacity ratio of these events can be seen in Fig. 9. The trap capacity was 37,000 m^3 and several 20,000 m^3 design events were tested with varying flood duration, grain size, and solid matter concentration. All were completely trapped (i.e., $V_* = V_{dep}/V_{supply} = 1$). The safety check with a 40,000 m^3-event fully filled the trap ($V_{dep} = V_{trap}$), but overwhelmed the trap capacity (i.e., $V_* < 1$). Overall, no sediment flushing was observed when mechanical clogging occurred in this large sediment detention basin.

5. Discussion

5.1. Self-flushing of hydraulic control barriers with bottom orifice - Comparison to previous observations

Partial self-flushing of hydraulic control barriers has actually been reported under three different conditions: (1) during receding hydrographs through slit check dams in the lab and in the field (Armanini & Larcher, 2001; Busnelli et al., 2001; Catella et al., 2005; Schwindt et al., 2018), (2) in the field because of a missing apron at the orifice bottom (Bezzola, 2008), or (3) in the lab during the rising limb of the hydrograph after the barrier experienced overflow, as in the current study (Fig. 7) and in Schwindt et al. (2018).

The first two conditions are similar to typical fan and delta morphodynamic processes, where deposition and erosion are controlled by the water level at the fan toe, i.e., the flooded part in the retention basin (Muto & Steel, 2004). Moreover, Schwindt et al. (2018) observed sediment flushing in an orifice dam reaching 140% of the peak sediment supply during short periods when the flood recession started. Such bursts of sediment releases are experienced when the water level drops at the delta-like deposit front, thus, enabling the formation of channel incision and the mobilization of previously submerged, trapped material as described by Piton & Recking (2016a).

The third condition is different since the sediment transport was re-established before the discharge started to recede. In Fig. 7, downstream sediment transport nearly equals the supply at the beginning of the experiment. This observation proves the guiding channel's capacity to convey low sediment discharge. When the water discharge increased ($Q_* \approx 1.35$ in Fig. 4), the sediment transport dropped to nearly zero and was later re-established. Moreover, the larger the trap retention capacity was, the later the sediment transport was re-established when the trap was full, but no true self-flushing (i.e., release of sediment that was actually trapped) was observed.

If the sediment transport was suddenly re-established before the flood recession started, it never exceeded the sediment supply for a long time. Under these conditions, the outlet transport rate was close to the supply rate, meaning that the sediment connectivity is simply recovered and the trap is merely transparent.

Fig. 9 summarizes the data of systematic experiments by Schwindt (2017), data from the current study, and observations from the Lancey case study by comparing the relative deposition volumes, $V_* = V_{dep}/V_{supply}$, with the relative supply volumes, $V_\Sigma * = V_{supply}/V_{trap}$. It can be observed that significant deposition occurred in both hydraulically controlled and hybrid barriers when the supply was much lower than the trap capacity (i.e., $V_\Sigma * << 1$). When the supplied volume approached the trap capacity, the relative deposition volume decreased more rapidly for

hydraulic than for hybrid control barriers, due to self-flushing of the hydraulic barriers. For supply volumes higher than the trap capacity ($V_\Sigma* > 1$), the relative deposition volume decreased to a small amount for hydraulic control and slightly less for hybrid barriers. For hydraulic barriers, this significant decrease was caused by flushing of previously deposited sediment. Conversely, for hybrid structures the supplied sediment was transported over the deposit, rendering the trap quasi-transparent to additional sediment supply once filled. A trap capacity equal to or larger than the maximum sediment supply volume expected during an event ($V_\Sigma * \ < 1$) should be chosen if possible.

5.2. Hybrid barrier and sediment size uncertainty

The sediment supply of mountain rivers may have various sources resulting in variable grain sizes (Piton & Recking, 2017; Rainato et al., 2016). Thus, the sediment size D_{95} is naturally subject to variation. The tests shown in Fig. 10 indicate that a hybrid barrier designed according to the recommendations of the generic study (i.e., with the estimated D_{95}) works correctly (gray lines in Fig. 10). However, if there is a risk of occurrence of an event with a much smaller grain size distribution than expected (e.g., activation of particular landslides) and there are no wood logs or boulders, the bar screen may not be clogged and the structure may malfunction. Indeed, it may result in a bar spacing of $b_\mathrm{i} > 1.34\ D_{95}$ and clearance heights of $a_\mathrm{mec} > 2.55\ D_{95}$, which proved to decrease the trapping efficiency (black line in Fig. 10). If such conditions are likely to occur (i.e., the total absence of logs and boulders and supply of large amounts of fine gravel), it is advisable to improve the robustness of the structure by increasing its overall capacity as previously mentioned (Fig. 9), and/or to store cobbles and boulders upstream of the barrier on the sides (beyond the banks) of the guiding channel.

In addition to the generic experiments, both the generic models and the case study done at the Artelia laboratory demonstrated that for an upstream reach supplying boulders (and eventually logs), a clearance height of $a_\mathrm{mec} \approx 1.5 - 1.6\ D_{95}$ and bar spacing $b_\mathrm{i} = 0.74 D_{95}$ worked as desired.

Schwindt et al. (2017) recommend to set b_i equal to $0.72 D_{95}$ and a clearance height of $a_\mathrm{mec} = 1.34 D_{95}$, which would result in a conservative design regarding the clogging probability. In light of the new tests (recommendation of $b_\mathrm{i} = 1.15 D_{95}$ and $a_\mathrm{mec} = 1.57 D_{95}$), these conservative values would also result in a higher likelihood of regular maintenance needs for clearing undesired deposition. It is worth noting that for the design of open Sabo dams made of steel pipes (although bars do not display a bottom clearance which is the innovative part of hybrid barrier and the reason why these experiments were required), there is also a general agreement that the interval should be about $1.5 - 2\ D_{95}$ to ensure high clogging probability (Itoh et al., 2011, 2013; Watanabe et al., 1980; Yuan et al., 2019).

6. Conclusions and practical recommendations

Bedload retention in sediment traps and the permeability of sediment control barriers are influenced by the basin geometry, barrier design, and the guiding channel across the deposition area. The current study introduces new aspects that enable improvement of the design procedure of check dams that are permeable for frequent floods and provide safe retention of sediment during hazardous events. This behavior is obtained through hybrid control barriers, which combine the hydraulically and mechanically controlled triggering of sediment retention. Compared with mechanically controlled barriers (i.e., open check dams with opening size close to grain size),

the hybrid control type is less vulnerable to grain size variation thanks to the added hydraulic control related to the orifice. At the same time, the bar screen of hybrid barriers prevents undesired self-flushing of sediment during floods as experienced with pure hydraulic control structures (e.g., slit dams). Hybrid control avoids undesired self-flushing and enables sediment passage during frequent floods owing to the bottom clearance below the bar screen, which is vital to avoid sediment starvation in downstream river reaches.
Provided that the basin retention capacity is sufficient to store the sediment volume of an event, a hybrid barrier with the following characteristics provides satisfactory performance: (i) a bottom orifice (slot) height slightly higher and larger than the guiding channel, a bar screen in front of the orifice with (ii) a bar spacing of approximately the characteristic grain size (0.75 - 1.15 D_{95}), and (iii) a bottom clearance height of 1.5-1.6 D_{95}. Values at the upper end of the given ranges of the bottom clearance height and bar spacing enhance sediment transfer during nonhazardous floods without reducing flood safety. Values at the lower end of the given ranges improve the reliability of retention of the structure in the case of strong uncertainty regarding the expected grain size distribution. Large woody debris enhances the clogging probability, and, therefore, the safety of hybrid control barriers. The resilience of the hybrid structure can be further enhanced by ensuring that the trap volume is larger than the total supply volume. Such designs prevent self-flushing even in the case of failure of mechanical blockage due to unexpectedly fine sediment supply, taking maximum advantage of the hybrid nature of the barrier.

Notation

The following symbols are used in this paper:

a	=	orifice height of slit check dam [m];
a_{mec}	=	bottom clearance height of the bar screen [m];
b	=	orifice width of slit check dam [m];
B	=	total barrier width [m];
b_{i}	=	bar spacing of the mechanical barrier [m];
$b_{\mathrm{i},*}$	=	relative bar spacing of the mechanical barrier ($b_{\mathrm{i},*} = b_{\mathrm{i}}/D_{95}$)[-];
D_{i}	=	diameter of which i percent of the sediment is smaller [m];
D_{95}	=	representative grain diameter [m];
Fr	=	Froude number [-];
f_{m}	=	relative bottom clearance height of the mechanical barrier ($f_{\mathrm{m}} = a_{\mathrm{mec}}/D_{95}$)[-];
g	=	gravitational acceleration [m/s^2];
h	=	flow depth [m];
m	=	channel bank inclination [-];
n	=	Manning´s roughness coefficient [m$^{-1/3}$s];
Q	=	discharge [m^3/s];
Q_*	=	discharge relative to the bankfull channel capacity [-];
$Q_{\mathrm{b,o}}$	=	sediment outflow [kg/s];
$Q_{\mathrm{b,i}}$	=	sediment supply [kg/s];
$Q_{\mathrm{b,max,1}}$	=	bedload transport capacity of the nonconstricted channel [kg/s];
$Q_{\mathrm{b,max,j}}$	=	bedload transport capacity at the flow constriction j [kg/s];
Q_{bf}	=	bankfull discharge of the guiding channel [m^3/s];

Q_{max} = maximum discharge possible in the model [m^3/s];
S_0 = channel slope [-];
s = specific gravity of sediment [-];
t = time, duration [s];
t_+ = duration of the rising hydrograph limb [s];
t_- = duration of the falling hydrograph limb [s];
t_* = relative duration ($t_* = t/t_+$) [-];
$V_{\sum *}$ = relative supply volume V_{supply}/V_{trap} [-];
V_{dep} = volume of sediment deposits [m^3];
V_{supply} = total supplied sediment volume during hydrograph [m^3];
V_{trap} = trap capacity, i.e., theoretical volume of the sediment trap [m^3];
w = bottom width of the guiding channel [m];
w_m = mean flow width of the guiding channel [m];
w_{basin} = width of the deposition area [m];
z_{dam} = barrier height [m];
α = first test run [-];
β = second test run (repetitive, redundant) [-];
λ = geometrical scale reduction [-];
ν = kinematic viscosity [m^2/s];
Φ_i = sediment supply intensity [-];
Φ_o = outflowing bedload intensity [-];
ρ_f = water density [kg/m^3];
ρ_s = sediment grain density [kg/m^3];
σ = width of the sediment grain size distribution [-] ($\sigma = 0.5\ (D_{84}/D_{50} + D_{50}/D_{16})$;
θ = normalized sediment transport [-] ($\theta = Q_{b,max,j}/Q_{b,max,1}$);

Data availability statement

Some or all data, models, or code generated or used during the study are available in a repository or online in accordance with funder data retention policies (Roth et al., 2019).

Acknowledgments

This work was funded by the Swiss Federal Office for the Environment (SFOEN) under the Sediment and Habitat Dynamics research project. The participation of G.P. was funded by the H2020 project NAIAD (NAture Insurance value: Assessment and Demonstration) [grant no. 730497] from the European Union's Horizon 2020 research and innovation program. The authors gratefully thank the Villard-Bonnot municipality and Artelia for allowing them to use the Combe de Lancey data and pictures.

References

Armanini, A., Dellagiacoma, F., & Ferrari, L. (1991). From the check dam to the development of functional check dams. In *Fluvial Hydraulics of Mountain Regions* (pp. 331–344). Berlin,

Heidelberg, Gemany: Springer-Verlag volume 37 of *Lecture Notes on Earth Sciences*. doi:10.1007/BFb0011200.

Armanini, A., & Larcher, M. (2001). Rational criterion for designing opening of slit-check dam. *Journal of Hydraulic Engineering*, *127*, 94–104. doi:10.1061/(ASCE)0733-9429(2001)127:2(94).

ARTELIA, & IRSTEA (2018). *Etude de l'aménagement d'une Plage de Dépôt sur le Torrent de la Combe De Lancey - Site des Anciennes Papèteries de Villard Bonnot - Rapport de Modélisation Physique*. Technical Report 8411764 Ville de Villard-Bonnot. (in French).

Badoux, A., Andres, N., & Turowski, J. (2014). Damage costs due to bedload transport processes in switzerland. *Natural Hazards and Earth System Sciences*, *14*, 279–294. doi:10.5194/nhess-14-279-2014.

Bergmeister, K., Suda, J., Hübl, J., & Rudolf-Miklau, F. (2009). *Schutzbauwerke gegen Wildbachgefahren: Grundlagen, Entwurf und Bemessung, Beispiele [Alpine flood protection: Planning basics, Design and Dimensioning, Examples]*. Berlin, Germany: Ernst & Sohn.

Bezzola, G. (2008). Unexpected processes in a sediment retention basin - the Stiglisbrücke basin on the Schächen torrent during the flood of August 2005. In *INTERPRAEVENT Conference Proceedings* (pp. 271–282). volume 1.

Bezzola, G. R., Sigg, H., & Lange, D. (2004). Schwemmholzrückhalt in der Schweiz [Driftwood retention in Switzerland]. In *Proceedings of INTERPRAEVENT* (pp. 29–40). Klagenfurt, Austria: International Research Society Interpraevent.

Busnelli, M. M., Stelling, G. S., & Larcher, M. (2001). Numerical Morphological Modeling of Open-Check Dams. *Journal of Hydraulic Engineering*, *127*, 105–114. doi:10.1061/(ASCE)0733-9429(2001)127:2(105).

Catella, M., Paris, E., & Solari, L. (2005). Case study: Efficiency of slit-check dams in the mountain region of versilia basin. *Journal of Hydraulic Engineering*, *131*, 145–152. doi:10.1061/(ASCE)0733-9429(2005)131:3(145).

Clauzel, L., & Poncet, A. (1963). Barrages filtrants et correction torrentielle par ségrégation des matériaux charriés. *Revue Forestière Française*, *4*, pp. 280 – 292. doi:10.4267/2042/24540. (In French).

Colar, R. (1970). Sul funzionamento delle briglie selettive. *Rassegna Tecnica del Friuli-Venezia Giulia*, (pp. 3–10). (In Italian).

D'Agostino, V. (2013). Filtering-retention check dam design in mountain torrents. In C. Garcia, & M. A. Lenzi (Eds.), *Check dams, morphological adjustments and erosion control in torrential streams* chapter 9. (pp. 185–210). New York: Nova Science.

D'Agostino, V., Degetto, M., & Righetti, M. (2000). Experimental investigation on open check dam for coarse woody debris control. *Dynamics of water and sediments in mountain basins, Quaderni di Idronomia Montana*, *20*, 201–212. BIOS, Cosenza, Italy.

Einstein, H. A. (1950). The Bed-Load Function for Sediment Transport in Open Channel Flows. *Technical Bulletin of the USDA Soil Conservation Service*, *1026*, 71.

Fedele, J. J., & Paola, C. (2007). Similarity solutions for fluvial sediment fining by selective deposition. *Journal of Geophysical Research*, *112*. doi:10.1029/2005jf000409.

Ferro, V. (2013). Modern strategies for torrent control: Slit and w-weir check dams. In C. Conesa-Garcia, & M. Lenzi (Eds.), *Check dams, morphological adjustments and erosion control in torrential streams* (pp. 33–62). Hauppauge, NY: Nova Science Publishers, Inc.

Horiguchi, T., & Richefeu, V. (2020). Post-analysis simulation of the collapse of an open sabo dam of steel pipes subjected to boulder laden debris flow. *International Journal of Sediment Research*, . doi:10.1016/j.ijsrc.2020.05.002.

Horiguchi, T., Shibuya, H., Katsuki, S., Ishikawa, N., & Mizuyama, T. (2015). A basic study on protective steel structures against woody debris hazards. *International Journal of Protective Structures*, *6*, 191–215. doi:10.1260/2041-4196.6.2.191.

Hübl, J. (2018). Conceptual framework for sediment management in torrents. *Water*, *10*, 1718. doi:10.3390/w10121718.

Huebl, J., & Fiebiger, G. (2005). Debris-flow mitigation measures. In M. Jakob, & O. Hungr (Eds.), *Debris-flow Hazards and Related Phenomena* chapter 18 - Debris-flow mitigation measures. (pp. 445–487). Springer Berlin Heidelberg. doi:10.1007/3-540-27129-5_18.

Ikeya, H. (1989). Debris flow and its countermeasures in Japan. *Bulletin of the International Association of Engineering Geology*, *40*, 15–33. doi:10.1007/BF02590339.

Itoh, T., Horiuchi, S., Akanuma, J.-I., Kaitsuka, K., Kuraoka, S., Morita, T., Sugiyama, M., & Mizuyama, T. (2011). Fundamental hydraulic flume tests focused on sediment control function using a grid-type high dam. *Italian Journal of Engineering Geology and Environment*, (pp. 1051–1061). doi:10.4408/IJEGE.2011-03.B-114.

Itoh, T., Horiuchi, S., Mizuyama, T., & Kaitsuka, K. (2013). Hydraulic model tests for evaluating sediment control function with a grid-type sabo dam in mountainous torrents. *International Journal of Sediment Research*, *28*, 511–522. doi:10.1016/S1001-6279(14)60009-3.

Kaitna, R., & Hübl, J. (2013). Silent witnesses for torrential processes. In M. Schneuwly-Bollschweiler, M. Stoffel, & F. Rudolf-Miklau (Eds.), *Dating torrential processes on fans and cones* (pp. 111–130). Dordrecht Heidelberg New York London: Springer volume 47. doi:10.1007/978-94-007-4336-6.

MacKenzie, L. G., Eaton, B. C., & Church, M. (2018). Breaking from the average: Why large grains matter in gravel-bed streams. *Earth Surface Processes and Landforms*, . doi:10.1002/esp.4465.

Muto, T., & Steel, R. J. (2004). Autogenic response of fluvial deltas to steady sea-level fall: Implications from flume-tank experiments. *Geology*, *32*, 401–404. doi:10.1130/G20269.1.

Piton, G., Carladous, S., Recking, A., Tacnet, J. M., Liébault, F., Kuss, D., Quefféléan, Y., & Marco, O. (2017). Why do we build check dams in Alpine streams? An historical perspective from the French experience. *Earth Surface Processes and Landforms*, *42*, 91–108. doi:10.1002/esp.3967.

Piton, G., Fontaine, F., Bellot, H., Liébault, F., Bel, C., Recking, A., & Hugerot, T. (2018a). Direct field observations of massive bedload and debris flow depositions in open check dams. In A. Paquier, & N. Rivière (Eds.), *E3S Web of Conferences* (pp. 1–8). EDP Sciences volume 40. doi:10.1051/e3sconf/20184003003.

Piton, G., Mano, V., Richard, D., Evin, G., Laigle, D., Tacnet, J., & Rielland, P. (2019). Design of a debris retention basin enabling sediment continuity for small events: the combe de lancey case study (france). In *Proc. 7th Int. Conf. on Debris-Flow Hazards Mitigation: Mechanics, Prediction, and Assessment* (pp. 1019–1026). doi:10.25676/11124/173113.

Piton, G., & Recking, A. (2016a). Design of Sediment Traps with Open Check Dams. I: Hydraulic and Deposition Processes. *Journal of Hydraulic Engineering*, *142*, 04015045. doi:10.1061/(ASCE)HY.1943-7900.0001048.

Piton, G., & Recking, A. (2016b). Design of Sediment Traps with Open Check Dams. II: Woody Debris. *Journal of Hydraulic Engineering*, *142*, 04015046. doi:10.1061/(ASCE)HY.1943-7900.0001049.

Piton, G., & Recking, A. (2017). The concept of travelling bedload and its consequences for bedload computation in mountain streams. *Earth Surface Processes and Landforms*, *42*, 1505–1519. doi:10.1002/esp.4105.

Piton, G., Recking, A., Le Coz, J., Bellot, H., Hauet, A., & Jodeau, M. (2018b). Reconstructing depth-averaged open-channel flows using image velocimetry and photogrammetry. *Water Resources Research*, *54*, 4164–4179. doi:10.1029/2017WR021314.

Rainato, R., Mao, L., Garcìa-Rama, A., Picco, L., Cesca, M., Vianello, A., Preciso, E., Scussel, G., & Lenzi, M. (2016). Three decades of monitoring in the rio cordon instrumented basin: Sediment budget and temporal trend of sediment yield. *Geomorphology*, *291*, 45–56. doi:10.1016/j.geomorph.2016.03.012.

Reneuve, P. (1955). L'évolution de la technique de correction torrentielle. *Revue Forestière Française*, (pp. 689–693). doi:10.4267/2042/27132. (in French).

Roth, A. (2017). Experimental Analysis of Bed Load Retention Mechanisms in Permeable Sediment Traps, . M.Sc. thesis, Hydraulic Constructions Platform PL- LCH, École Polytechnique Fédérale de Lausanne EPFL.

Roth, A., Piton, G., Schwindt, S., Jafarnejad, M., & Schleiss, A. (2019). rothanita/data-sediment-trap: Journal submission. Zenodo. doi:10.5281/zenodo.3240601.

Schwindt, S. (2017). Hydro-morphological processes through permeable sediment traps at mountain rivers. *Communication (Laboratoire de constructions hydrauliques, Ecole polytechnique fédérale de Lausanne). 71*, *Ed. Anton Schleiss*. doi:10.5075/epfl-lchcomm-71. (PhD Thesis No. 7655).

Schwindt, S., Franca, M. J., De Cesare, G., & Schleiss, A. J. (2017). Analysis of mechanical-hydraulic deposition control measures. *Geomorphology*, *Vol. 295*, pp. 467–479. doi:10.1016/j.geomorph.2017.07.020.

Schwindt, S., Franca, M. J., Reffo, A., & Schleiss, A. J. (2018). Sediment traps with guiding channel and hybrid check dams improve controlled sediment retention. *Natural Hazards and Earth System Sciences*, *18*, 647–668. doi:10.5194/nhess-18-647-2018.

Schwindt, S., Franca, M. J., & Schleiss, A. J. (2019). Bottom slope influence on flow and bedload transfer through contractions. *Journal of Hydraulic Research*, *Vol. 57*, pp. 197–210. doi:10.1080/00221686.2018.1454519.

Shima, J., Moriyama, H., Kokuryo, H., Ishikawa, N., & Mizuyama, T. (2016). Prevention and Mitigation of Debris Flow Hazards by Using Steel Open-Type Sabo Dams. *International Journal of Erosion Control Engineering*, *9*, 135–144. doi:10.13101/ijece.9.135.

Shima, J., Yoshida, K., Kawakami, Y., & Mizuyama, T. (2015). Consideration on boulders & members' interval of open type steel sabo dam for capturing debris flow. *Journal of the Japan Society of Erosion Control Engineering*, *67*. doi:10.11475/sabo.67.5_3.

Smart, G. M. (1984). Sediment Transport Formula for Steep Channels. *Journal of Hydraulic Engineering*, *110*, pp. 267–276. doi:10.1061/(ASCE)0733-9429(1984)110:3(267).

Tateishi, R., Horiguchi, T., Sonoda, Y., & Ishikawa, N. (2020). Experimental study of the woody debris trapping efficiency of a steel pipe, open sabo dam. *International Journal of Sediment Research*, *35*, 431–443. doi:10.1016/j.ijsrc.2020.03.011.

Watanabe, M., Mizuyama, T., & Uehara, S. (1980). Review of debris flow countermeasure facilities. *Journal of the Japan Erosion Control Engineering Society*, *115*, 40–48.

Yalin, M. S. (1977). *Mechanics of sediment transport* volume 2. Oxford and New York: Pergamon Press Oxford.

Yuan, D., Liu, J., You, Y., Zhang, G., Wang, D., & Lin, Z. (2019). Experimental study on the performance characteristics of viscous debris flows with a grid-type dam for debris flow hazards mitigation. *Bulletin of Engineering Geology and the Environment*, *78*, 5763–5774. doi:10.1007/s10064-019-01524-z.

Zollinger, F. (1984). Die verschiedenen Funktionen von Geschieberückhaltebauwerken [The different functions of debris retention dams]. In *Proceedings of INTERPRAEVENT* (pp. 147–160). Klagenfurt, Austria: International Research Society Interpraevent. URL: http://www.interpraevent.at/palm-cms/upload_files/Publikationen/Tagungsbeitraege/1984_1_147.pdf.